NASA/TM—2011-216769/PART1 GT2010–22825

Results of an Advanced Fan Stage Operating Over a Wide Range of Speed and Bypass Ratio

Part 1: Fan Stage Design and Experimental Results

Kenneth L. Suder
Glenn Research Center, Cleveland, Ohio

Patricia S. Prahst
AP Solutions, Inc., Cleveland, Ohio

Scott A. Thorp
Glenn Research Center, Cleveland, Ohio

October 2011

NASA STI Program . . . in Profile

Since its founding, NASA has been dedicated to the advancement of aeronautics and space science. The NASA Scientific and Technical Information (STI) program plays a key part in helping NASA maintain this important role.

The NASA STI Program operates under the auspices of the Agency Chief Information Officer. It collects, organizes, provides for archiving, and disseminates NASA's STI. The NASA STI program provides access to the NASA Aeronautics and Space Database and its public interface, the NASA Technical Reports Server, thus providing one of the largest collections of aeronautical and space science STI in the world. Results are published in both non-NASA channels and by NASA in the NASA STI Report Series, which includes the following report types:

- TECHNICAL PUBLICATION. Reports of completed research or a major significant phase of research that present the results of NASA programs and include extensive data or theoretical analysis. Includes compilations of significant scientific and technical data and information deemed to be of continuing reference value. NASA counterpart of peer-reviewed formal professional papers but has less stringent limitations on manuscript length and extent of graphic presentations.

- TECHNICAL MEMORANDUM. Scientific and technical findings that are preliminary or of specialized interest, e.g., quick release reports, working papers, and bibliographies that contain minimal annotation. Does not contain extensive analysis.

- CONTRACTOR REPORT. Scientific and technical findings by NASA-sponsored contractors and grantees.

- CONFERENCE PUBLICATION. Collected papers from scientific and technical conferences, symposia, seminars, or other meetings sponsored or cosponsored by NASA.

- SPECIAL PUBLICATION. Scientific, technical, or historical information from NASA programs, projects, and missions, often concerned with subjects having substantial public interest.

- TECHNICAL TRANSLATION. English-language translations of foreign scientific and technical material pertinent to NASA's mission.

Specialized services also include creating custom thesauri, building customized databases, organizing and publishing research results.

For more information about the NASA STI program, see the following:

- Access the NASA STI program home page at *http://www.sti.nasa.gov*

- E-mail your question via the Internet to *help@sti.nasa.gov*

- Fax your question to the NASA STI Help Desk at 443–757–5803

- Telephone the NASA STI Help Desk at 443–757–5802

- Write to:
  NASA Center for AeroSpace Information (CASI)
  7115 Standard Drive
  Hanover, MD 21076–1320

NASA/TM—2011-216769/PART1 GT2010–22825

Results of an Advanced Fan Stage Operating Over a Wide Range of Speed and Bypass Ratio

Part 1: Fan Stage Design and Experimental Results

Kenneth L. Suder
Glenn Research Center, Cleveland, Ohio

Patricia S. Prahst
AP Solutions, Inc., Cleveland, Ohio

Scott A. Thorp
Glenn Research Center, Cleveland, Ohio

Prepared for the
Turbo Expo 2010
sponsored by the American Society of Mechanical Engineers (ASME)
Glasgow, Scotland, United Kingdom, June 14–18, 2010

National Aeronautics and
Space Administration

Glenn Research Center
Cleveland, Ohio 44135

October 2011

Acknowledgments

Authors would like to acknowledge General Electric (GE) personnel: Peter Wood and Mark Mielke for the many helpful discussions related to the fan stage design and their insights into the interpretation of the experimental and computational results. Additional acknowledgement to Dr. Aamir Shabbir of United Technologies Research Center (UTRC), Rick Mulac from the University of Toledo, Dr. John Adamczyk (NASA retired), and Tim Beach from AP Solutions for their support and efforts related to the APNASA flow simulations. Without these acknowledged contributions the work presented in this paper would not have been possible.

Trade names and trademarks are used in this report for identification only. Their usage does not constitute an official endorsement, either expressed or implied, by the National Aeronautics and Space Administration.

This work was sponsored by the Fundamental Aeronautics Program at the NASA Glenn Research Center.

Level of Review: This material has been technically reviewed by technical management.

Available from

NASA Center for Aerospace Information
7115 Standard Drive
Hanover, MD 21076–1320

National Technical Information Service
5301 Shawnee Road
Alexandria, VA 22312

Available electronically at http://www.sti.nasa.gov

Results of an Advanced Fan Stage Operating Over a Wide Range of Speed and Bypass Ratio
Part 1: Fan Stage Design and Experimental Results

Kenneth L. Suder
National Aeronautics and Space Administration
Glenn Research Center
Cleveland, Ohio 44135

Patricia S. Prahst
AP Solutions, Inc.
Cleveland, Ohio 44135

Scott A. Thorp
National Aeronautics and Space Administration
Glenn Research Center
Cleveland, Ohio 44135

Abstract

NASA's Fundamental Aeronautics Program is investigating turbine-based combined cycle (TBCC) propulsion systems for access to space because it provides the potential for aircraft-like, space-launch operations that may significantly reduce launch costs and improve safety. To this end, National Aeronautics and Space Administration (NASA) and General Electric (GE) teamed to design a Mach 4 variable cycle turbofan/ramjet engine for access to space. To enable the wide operating range of a Mach 4+ variable cycle turbofan ramjet required the development of a unique fan stage design capable of multi-point operation to accommodate variations in bypass ratio (10×), fan speed (7×), inlet mass flow (3.5×), inlet pressure (8×), and inlet temperature (3×). In this paper, NASA has set out to characterize a TBCC engine fan stage aerodynamic performance and stability limits over a wide operating range including power-on and hypersonic-unique "windmill" operation. Herein, we will present the fan stage design, and the experimental test results of the fan stage operating from 15 to 100 percent corrected design speed. Whereas, in the companion paper (Ref. 1), we will provide an assessment of NASA's APNASA code's ability to predict the fan stage performance and operability over a wide range of speed and bypass ratio.

Introduction

Studies performed under NASA's Next Generation Launch Technology Program and the NASP High Speed Propulsion Assessment (HiSPA) program indicated a variable cycle turbofan/ramjet was the best configuration to satisfy access-to-space mission requirements for the first stage of a two-stage-to-orbit system because this configuration maximizes the engine thrust-to-weight ratio while minimizing frontal area (Ref. 2). To this end, NASA and GE teamed to design a variable cycle engine for an aircraft launch vehicle with Mach 4+ capability for access to space (Refs. 3 and 4). The flight envelope of a Mach 4+ like space launch vehicle operating from runway takeoff with continuous acceleration through transition from turbofan to ramjet operation requires a turbofan engine with wide operating range capability. To enable the wide operating range of a Mach 4+ variable cycle turbofan ramjet required the development of a unique fan stage design capable of multi-point operation which provided high pressure ratio and efficiency at takeoff through the mid range of engine operation, while avoiding stall and minimizing losses at the higher flight Mach numbers.

To mitigate the risk of meeting the unique design requirements for the fan stage, NASA and GE teamed to design and build a 57 percent engine scaled fan stage to be tested in NASA's transonic compressor facility. The goals of this test were to assess the aerodynamic and aero mechanic performance and operability characteristics of the fan stage over its required range of operation from 15 to 100 percent fan corrected speed.

The objectives of this research activity was to assess and document the capability of state-of-the art design and analysis tools (validated for subsonic flight vehicles) to design and predict the performance and operability of an advanced fan stage designed to meet the requirements for the first stage of a two-stage-to-orbit hypersonic vehicle (i.e., necessitating wide multi-point operating range). These design and analysis tools are still relevant because the inlet has diffused the fan axial Mach number to subsonic, however the wide operating range and advanced configurations required for a Mach 4+ vehicle result in using these tools beyond the operating ranges these tools were validated. The ultimate goal being able to have confidence in the tools to design and analyze these advanced TBCC configurations to meet future mission requirements.

In the following sections we will describe the fan stage design, the experimental facility and instrumentation, a sampling of test results to highlight the fan stage performance

and operability characteristics, the pre-test CFD predictions and comparison to the experimental results, and conclude with a summary of lessons learned and rationale for additional post-test CFD simulations to assess the ability of our tools to predict the fan stage performance and operability. These post-test simulations will be presented in Part 2 of this paper (Ref. 1) and will include additional detailed comparisons of the simulations to the experimental results.

Fan Stage Design

An overview of the fan stage design requirements and traceability to a Mach 4 TBCC engine propulsion system is provided in References 3 to 6 where it is shown that the fan stage is a critical enabling component for the Mach 4 TBCC engine. The fan stage flow-path and components shown in Figure 1 are a 22 in. diameter scaled simulation of the engine (38 in. diameter) fan stage and includes the fan rotor, outlet guide vane (OGV), and splitter flow-path including the engine frame struts. To enable the wide operating range of the Mach 4+ capable engine required the development of a unique fan stage design for multi-point operation to accommodate variations in bypass ratio (10×), fan rotor speed (7×), inlet mass flow (3.5×), inlet pressure (8×), and inlet temperature (3×). Herein, bypass ratio is defined as the ratio of mass flow in the bypass duct to that in the core duct (see Fig. 1).

These large variations of the inlet conditions and rotational speed introduced the following aerodynamic technical challenges to the fan stage design:

1. Stall Free operation of the fan stage from 15 to 110 percent rotor design speed (corrected).
2. Minimize the pressure losses through the fan rotor and OGV especially at the very high bypass ratios where the fan stage is at or approaching "windmill" conditions.
3. Avoid choking and provide clean and stable flow in the bypass and core ducts throughout the 10× range of bypass ratio.
4. Deliver the required inlet conditions to the downstream engine components (ramjet and core compressor), from takeoff through transonic and to ramjet operation.

These technical challenges were augmented by the requirement to maintain traceability to the reference TBCC vehicle which resulted in 1) a fan stage design without inlet guide vanes; thereby, making it more difficult to maintain performance and operability over the wide operating range, and 2) a bypass duct arrangement that must maintain a diameter consistent with scale-up to the reference vehicle, yet not be so small as to incur huge pressure losses or potential flow choking resulting from high Mach numbers in the duct. Overall fan stage performance and operability therefore requires major consideration, as competing goals at different operating points become major drivers in the design. A summary of the fan stage design features is found in Table 1

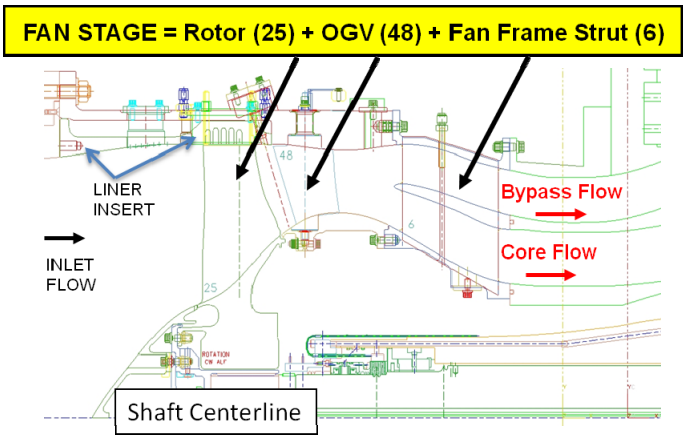

Figure 1.—Fan stage components and flow path.

TABLE 1.—SELECTED FAN STAGE DESIGN PARAMETERS

Fan rotor airfoils	25
Tip speed at 17280 rpm	506 m/s (1660 ft/s)
Radius ratio at LE	0.43
Avg. aspect ratio	1.12
Avg. solidity	2.2
Tip clearance/chord	~0.009 nominal
Specific flow	38.0
OGV airfoils	48
Design flow rate	37.3 kg/s (82 lbm/s)
Stage PR	2.47
Stage adiabatic efficiency	85.7
Stall margin—high speed	12%
Stall margin—low speed	20%

and the resulting geometry for the fan and OGV are shown in Figure 2. The details of the mechanical design and aeromechanic test data are found in References 5 and 7, respectively.

Fan Rotor Design

The fan stage was designed by GE engineers following their standard design practice, with close collaboration from NASA engineers providing multi-stage CFD analysis in support of the design. The fan rotor was designed to produce a high pressure ratio (2.5) at lower flight Mach numbers while maintaining adequate stall margin (>10 percent) across a wide range of operating conditions. In order to deliver the required performance, an advanced technology, forward swept fan rotor design (Refs. 5 to 7) was employed. The resulting fan rotor geometry is shown in Figure 2(a).

The fan stage design operating line (as determined by GE's cycle code to meet mission requirements) is depicted by the black line connecting the black circles in Figure 3. CFD simulations were used to update the fan stage performance maps in the engine cycle deck. Single blade row CFD analyses were run using GE's TACOMA (Ref. 8) code along the operating line at 100, 90, 80, 50, 37, 20, and 15 percent of design speed, as well as near stall at 100 and 80 percent speed.

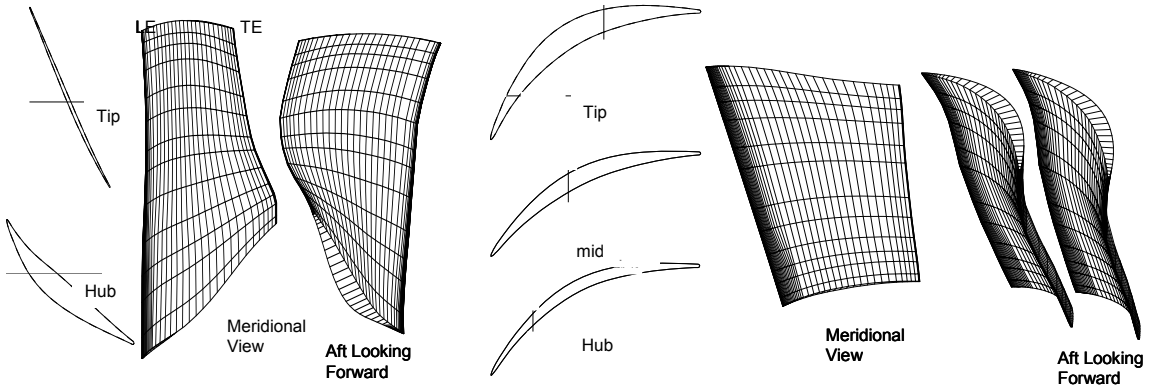

a) Advanced technology forward swept fan

b) OGV bowed and leaned at the hub to turn air into the core.

Figure 2.—Fan and OGV design airfoil shapes.

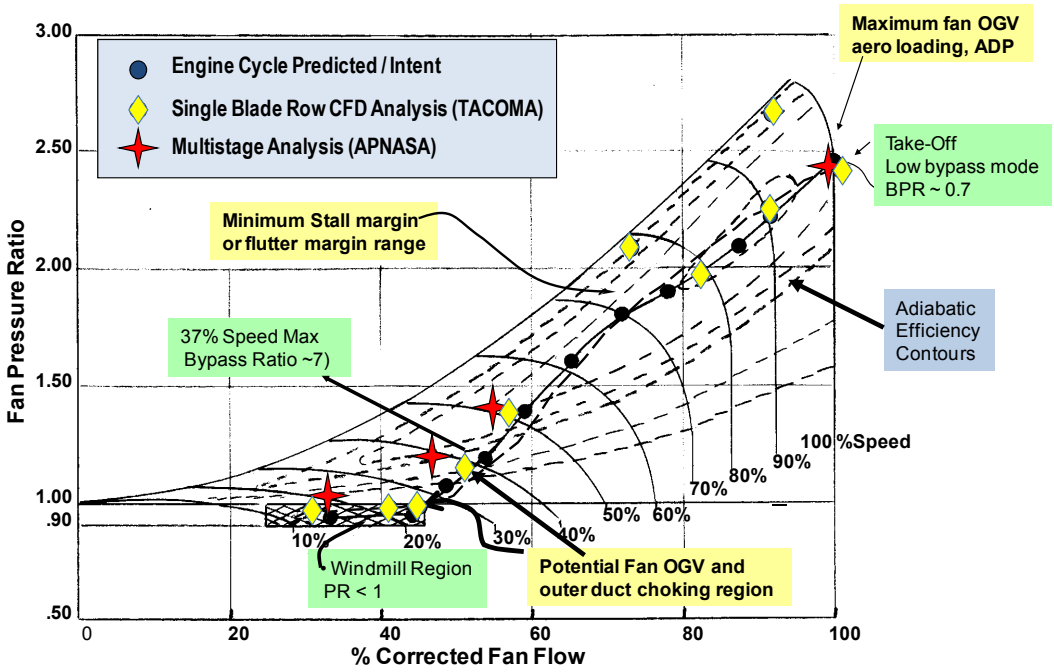

Figure 3.—Fan stage operating map—design operating line.

Multi-stage CFD analyses were also conducted at select operating conditions (100, 50, and 37 percent of design speed), utilizing NASA's APNASA (Ref. 9) code. These simulations predict that the fan stage should be capable of matching the design intent across the operating range. In order to insure adequate stall margin over the operating range, the fan stage test article provided the flexibility to incorporate various casing treatments over the fan rotor by installing a liner insert as depicted in Figure 1. Three liners were designed and tested with the fan stage: one smooth liner with a nominal fan tip clearance and 2 liners with identical circumferential grooves of which one had the same clearance as the smooth liner and the other with twice the clearance, herein designated open clearance. The 5 circumferential grooves over the rotor tip (see Fig. 1) have an axial width to radial height ratio of approximately 0.4 and are centered at 10, 25, 40, 55, and 70 percent axial rotor chord. The sensitivity of stage performance and operability to liner configuration will be presented in the experimental results.

OGV Design

The OGV airfoil design is very three-dimensional, with significant amounts of bow and lean at the hub, both to strengthen the endwall flow and to help turn air into the engine core duct. The resulting geometry for the fan and OGV are shown in Figure 2. Along the operating line, shown in Figure 3, the mission requires the fan to operate at near peak efficiency at design speed (i.e., highly loaded operation), but near the maximum flow at 15 to 37 percent design speed

(lightly loaded operation). Note that this operating line is unique to the hypersonic mission in that the fan bypass and core streams are independently throttled using a variable nozzle in each stream; thereby resulting in an operating line very much different from a fan operating line generated using a variable or fixed nozzle. Therefore, along the required fan operating line, the fan loading and (work factor) decreases with fan rotational speed which reduces the tendency of the fan rotor to stall at the lower speeds, but produces lower air angle onto the downstream OGV. At the aerodynamic design point (ADP), the OGV is heavily loaded and operates with high inlet air angles and Mach numbers, thereby resulting in high solidity to avoid the risk of stall. Quantitative values indicative of the OGV incidence and inlet Mach number will be presented in the experimental results session.

The original design intent was to have a fixed OGV to minimize weight and complexity and minimize the clearance between the OGV and the endwalls. However, these large swings of incidence to the OGV over the 15 to 100 percent speed operating range, create significant aerodynamic design challenges resulting in the necessity for a variable OGV. To illustrate this point, the mid-span flow field of the OGV was analyzed using a two-dimensional CFD (2D-TACOMA) code (Ref. 8) at 37 percent design speed for the OGV setting angle of 0° (i.e., the baseline setting angle at the ADP) and a more open setting angle of 10°. These results, plotted in Figure 4, show that if the OGV was fixed at the 0° setting angle over the operating range, the high negative incidences onto the vane causes the pressure surface to separate. This in turn creates additional blockage through the vane creating a choking problem which would not only restrict flow to the downstream engine components and reduce thrust but also would impact the ability to move the fan operating point with downstream variable geometry. For the 10° open setting angle, these OGV flow field simulations, shown in Figure 4, illustrates the OGV still has a small but very limited flow separation off the pressure surface. To open the OGV further would reduce the flow separation at the expense of increasing endwall clearance and compromising design speed performance.

Figure 5 compares the flow field solution (obtained from the three-dimensional N-S APNASA code (Ref. 9)) for the OGV design at 100 percent speed (0° setting angle) to the results at

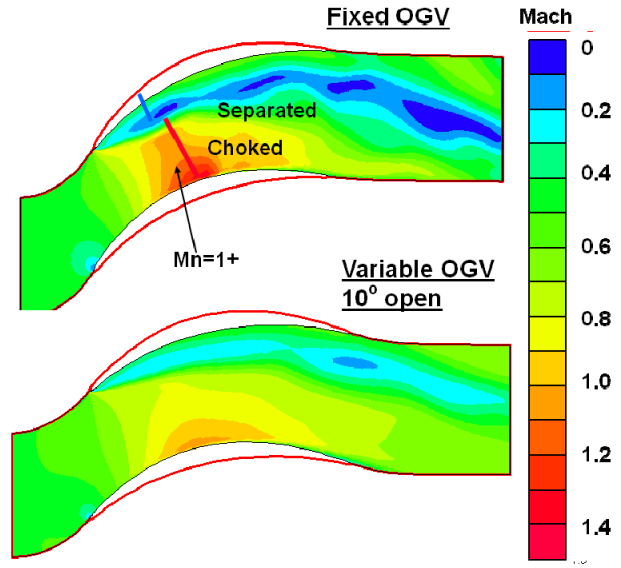

Figure 4.—Two-dimensional CFD (TACOMA) simulation of the OGV flow field at 50 percent span and 37 percent speed.

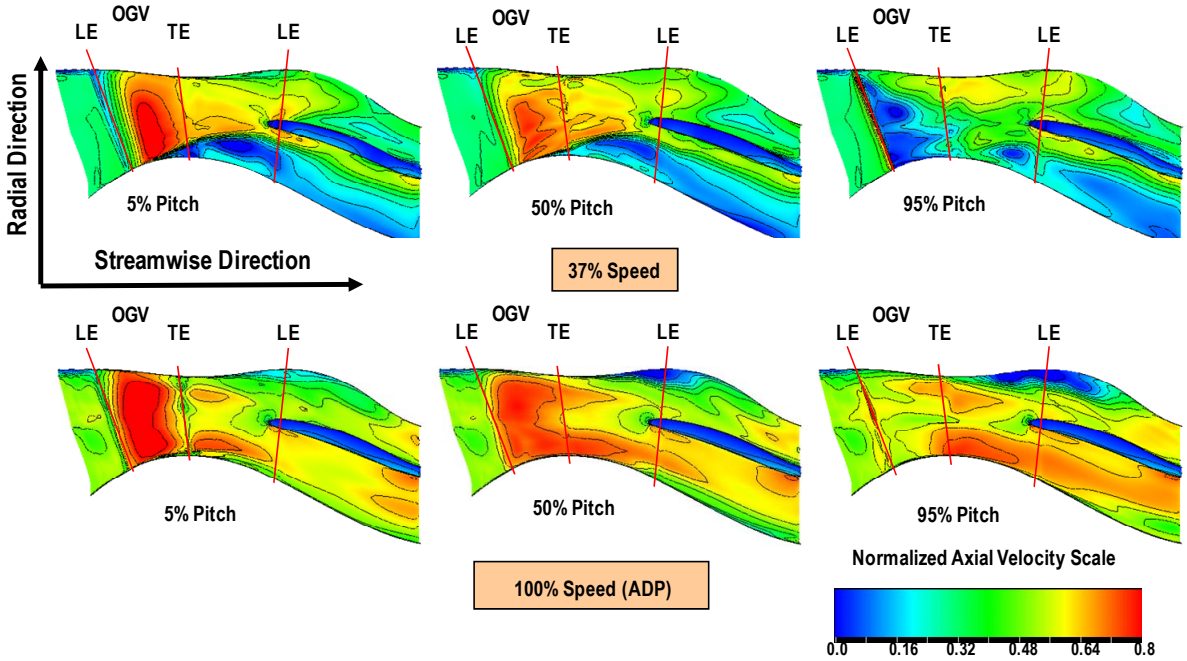

Figure 5.—APNASA simulations of the OGV flow field at 100 and 37 percent speed for the fixed and open OGV settings.

37 percent speed with the OGV rotated 10° open. At 100 percent design speed the OGV core flow field is well behaved, but the bypass duct flow field exhibits regions of low axial momentum in the bypass duct which results from the area increase and resulting diffusion in the bypass duct. Whereas, at 37 percent speed the opposite occurs in that the OGV flow field provides low axial momentum flow in the engine core duct, and the bypass duct flow is well behaved. The extremely low velocity in the lower spans of the OGV is required to obtain the high bypass ratio required for the cycle. Therefore, the final OGV design balances competing requirements over the entire range of operation by minimizing losses in the core duct at 100 percent speed where the bypass ratio is low and the engine thrust is derived mainly from the engine core, and it passes the flow without choking the bypass duct or incurring massive separations in the core duct where the bypass ratio is high and the thrust is derived mainly from the bypass flow. In summary, the final stage design satisfied its performance and operability requirements along the entire operating line. Through careful flow path and airfoil design, both single blade row and multistage CFD analyses showed that these requirements could be met. In the remainder of the paper, the experimental results will compare the measured performance to the design intent and show quantitatively the compromises in performance resulting from operating over such a wide operating range.

Experimental Setup

The NASA Single-Stage Axial Compressor Facility, illustrated in Figure 6, was used to investigate the aerodynamic performance of this compressor. The drive system consists of a 7,000 hp, 3,600 rpm electric drive motor and a 7,000 hp speed-increasing gearbox with a gear ratio of 5.9, powered by the Engine Research Building (ERB) Variable Frequency system. The compressor speed can be controlled between 1,860 and 21,240 rpm. An in-line torque meter rated for 22,000 in.-lb measures power absorbed by the research compressor. The test rig shafting is bored to provide the capability for rotating measurements using a 100 channel slip ring.

The facility air system is sized for a maximum flow of 100 lbm/s. Atmospheric air is drawn into the facility, passes through a filter, through a flow measuring orifice plate, through inlet control valves, and into the plenum chamber. The plenum contains flow conditioning to provide an inlet flow turbulence intensity of 1.5 percent at the bell-mouth entrance and <1 percent at the fan rotor. The mass flow rate through the bypass and core ducts (refer to Fig. 1) is independently controlled by two throttle valves downstream of the fan stage. Air discharged from the exhaust collector is cooled by water spray injection and exhausted to atmosphere or via the altitude exhaust system. The altitude exhaust capability is a key feature of this facility which enabled mapping of fan stage operation at 50 percent design speed

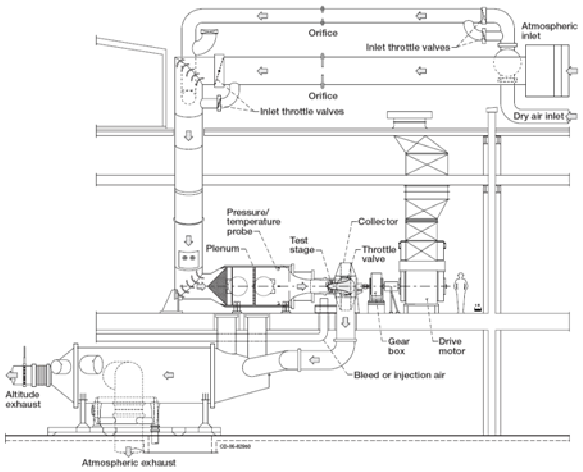

Figure 6.—NASA Single Stage Compressor Facility.

and below where the fan stage pressure ratio is near or below 1.0 (i.e., referred to as "windmill" condition in the context of this paper).

Instrumentation

Rig aerodynamic instrumentation was designed to capture flow details of interest and a schematic is presented in Figure 7. Full details of the instrumentation package can be found in References 5 and 10. In order to capture the inlet flow field, inlet rakes were placed at the bell-mouth exit. These rakes were placed well upstream of the fan to reduce the risk of potentially harmful aeromechanical interaction between these large rakes and the fan. High response pressure transducers and matching static pressure taps were placed in an axial array over the fan tip to allow mapping of the shock structure in this region, as a function of speed and throttle position. Six OGV leading edges were instrumented with radial arrays of total temperature and total pressure sensors to evaluate fan performance. Overall stage performance measurements were made with rakes located downstream of the OGV before the flow split (refer to Fig. 7). Eight rakes were clocked around the circumference with no more than one rake per OGV passage which could be reconstructed to measure across one OGV pitch (see the inset in Fig. 7). Each rake consisted of 7 radial elements at 8, 24, 39, 53, 67, 81, and 94 percent spans (equal areas) measured both total pressure and temperature. Static pressures were measured at the hub and case location coinciding with the measurement plane of each rake and were used to quantify stage performance. The OGV's were also instrumented with static pressure taps at 4 span-wise locations (10, 15, 25, and 45 percent span from the hub) from vane leading to trailing edge on both pressure and suction surfaces. These static taps were used to assess OGV blade loading as well as characterize the incidence angle on the OGV. Boundary layer and total temperature and pressure combination rakes were placed in the bypass and core ducts downstream of the splitter, both to determine duct and strut

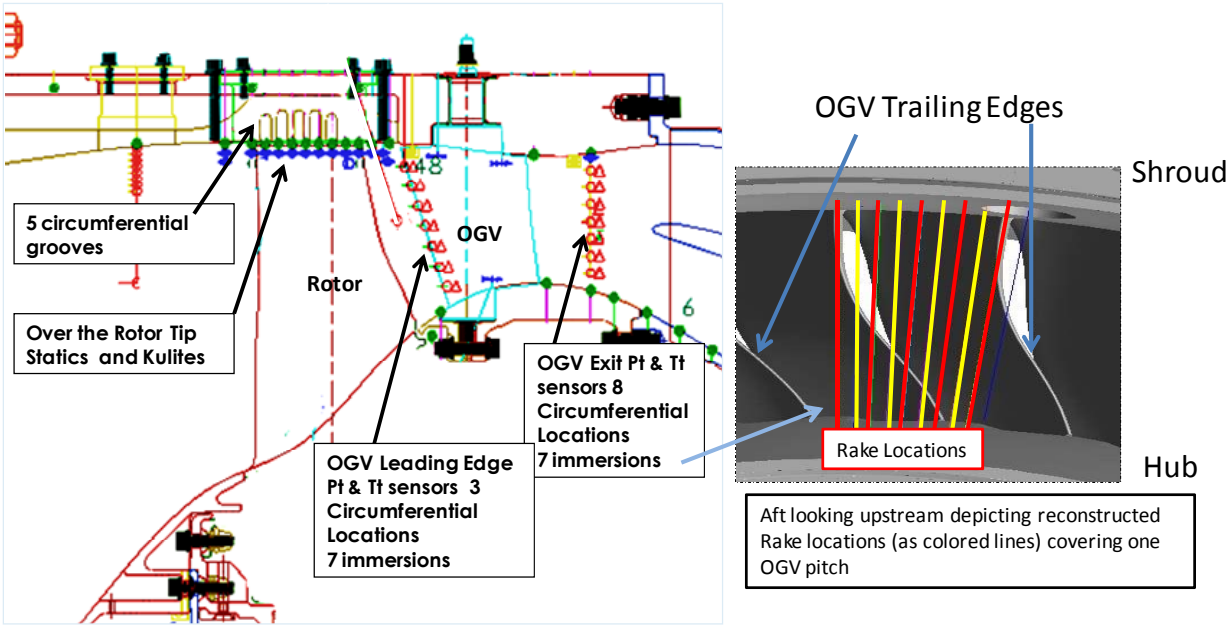

Figure 7.—Instrumentation schematic for fan stage used to obtain stage performance and operability.

losses as well as to measure the mass flow rate in each stream so that the required operating bypass ratio could be set. Finally, static pressure taps were distributed along the flow-path in several critical regions to detect separated flow.

Test Procedure

Initial testing focused on defining the safe zones of operation and entailed mapping the operating line over the speed range. To limit the number of stalls, additional mapping from the operating line to the stall line were acquired while monitoring operability Kulites for aerodynamic stall and light probes, accelerometers, and strain gages for mechanical and aeromechanical stability. If any of these instruments indicated we were approaching and aerodynamic or aeromechanical instability the mapping was stopped and returned to the operating line. This procedure was used for the smooth liner and grooved liner with nominal clearance configurations, but for the grooved liner large clearance (2 times nominal) all but 4 of the strain gages were inoperable and it was decided to only go to the same operating conditions that were cleared during the testing of the previous 2 liners. The aeromechanic results are documented in Reference 5 and show that the fan stage is safe to operate anywhere along the operating line. Furthermore, the aeromechanic results in Reference 5 show the fan stage can operate over the entire operating range without endwall casing treatment because the stage stalls aerodynamically prior to reaching aeromechanical stability limits (i.e., flutter boundaries). However, with casing treatment the aerodynamic stability limit and aeromechanical stability limit (stall flutter boundary) overlap and therefore limited near stall data were acquired with casing treatment configurations. In all cases the speed lines were mapped to very near aerodynamic stall conditions.

In order to obtain data for a speed line, the pressure ratio, mass flow, and bypass ratio were set to match the design intent along the operating line. Initially, the intent was to map a speed line at constant bypass ratio. However, once testing began it was clear that manually adjusting the throttle valve for each of the bypass and core ducts would be too time consuming. Therefore, the speed lines were acquired by initiating at the operating line condition and then by first moving the bypass valve while maintaining a fixed position on the core duct throttle valve and second by returning to the operating line and closing the core duct valve while maintaining a fixed position on the bypass throttle valve. This process enabled full mapping from maximum flow to near stall condition at a given speed but does result in a slight variation of bypass ratio along the speed line. In all instances the maps at a given speed line will be presented with the data obtained with the bypass ratio closest to the bypass ratio of the design intent along the operating line. In the companion paper (Ref. 1), the sensitivity of the fan stage performance to slight variations in bypass ratio will be presented.

Experimental Results

Aerodynamic fan stage performance characteristics were acquired at 15, 25, 37, 50, 60, 70, 80, 85, 90, 95, 100, and 101 percent of design rotor speed for three different fan rotor casing configurations corresponding to 1) smooth wall at nominal clearance, 2) circumferentially grooved casing at nominal clearance and 3) circumferentially grooved casing at twice nominal tip clearance. Nominal tip clearance was

measured to be 0.005 of tip chord (design value = 0.009) at fan mid-chord at 100 percent speed; whereas, the open clearance was measured to be 0.018 of tip chord at 100 percent speed. Uncertainty analysis was performed on the measured and relevant calculated parameters. The uncertainties actually vary for every measured data point; however, at a given rotational rotor speed the uncertainties remain nearly constant. The nominal data uncertainties for each speed are provided in Table 2. Only selected data are presented to highlight the features of the wide operating design requirements for this stage. For example, in the following sections we will discuss the impact of the liner configuration and OGV setting angle on the stage performance. Radial profiles of the total pressure ratio at 100 percent speed are presented to indicate the distribution of OGV losses. Additional radial profiles will be presented in Part 2 of this paper to make detailed comparisons with the CFD simulations.

TABLE 2.—NOMINAL DATA UNCERTAINTIES

DATA Uncertainties					
% Rotational Speed	100%	90%	80%	60%	37%
MassFlow (kg/sec)	0.15	0.16	0.19	0.23	0.03
PR	0.008	0.008	0.008	0.008	0.008
Efficiency	0.005	0.006	0.008	0.014	0.03
Stall MassFlow (kg/sec)	0.15	0.16	0.19	0.23	0.03
Stall PR	0.008	0.008	0.008	0.008	0.008
StallMargin (%)	0.40%	0.50%	0.70%	1.10%	0.20%

Measured Speed Lines and Comparison With Design Intent

Experimental results of the fan stage characteristics at 15, 25, 37, 50, 60, 70, 80, 85, 90, 95, and 100 percent of rotor design speed are shown in terms overall stage pressure ratio and adiabatic efficiency for the smooth wall configuration in Figure 8. The speed-lines are being shown for smooth wall nominal clearance (0.012 in. at 100 percent speed varying to 0.026 in. at 50 percent speed and below). The black line in the pressure ratio plot represents the design operating line for the compressor and the red line indicates the notional aerodynamic stall line as estimated from GE's design procedure. Note that the uncertainties in pressure ratio and mass flow are within the symbol size. The uncertainty in efficiency varies dramatically with speed (Table 2) primarily because the work done on the fluid diminishes rapidly with rotational speed and the uncertainty in temperature measurement results in greater uncertainties in efficiency at the lower speeds. Also note the efficiency at 15 percent speed is not shown because at this speed the stage pressure ratio is less than 1 and stage losses are greater than the work added to the fluid by the rotor and therefore the meaning of efficiency (ratio of energy added to the fluid to the energy input to drive the fan rotor) is invalid. For simplicity the data presented hereafter, will not include the error bars. The overall performance characteristics of the fan stage for the grooved liner with nominal and open clearances are provided in Figures 9 and 10.

The data point corresponding to the lowest value of corrected flow for each speed-line does not necessarily correspond to the aerodynamic stall point. If an aerodynamic stall was obtained, it is shown by the solid red filled symbol data point as indicated in the pressure ratio plot for the speed-lines of 95, 90, 85, 80, 70, 50, and 37 percent of fan rotational speed. As can be seen from Figure 8, 100 percent speed was not throttled to an aerodynamic stall, instead an audible hum was observed. Data from the strain gages, light probes, and Kulite data indicated the hum was not associated with an increase in fan stage mechanical stress nor of that for a typical rotating stall. However the operability Kulite measurements exhibited an increase in unsteadiness at the last data point acquired at 100 percent speed in Figure 8 for the smooth wall configuration consistent with those observed at a near stall operating condition.

Detailed comparison of measured performance along the operating line from 15 to 100 percent speed is shown in Figure 11. It is evident the stage design met its design intent not only in pressure rise and efficiency but also in flow rate and stall margin.

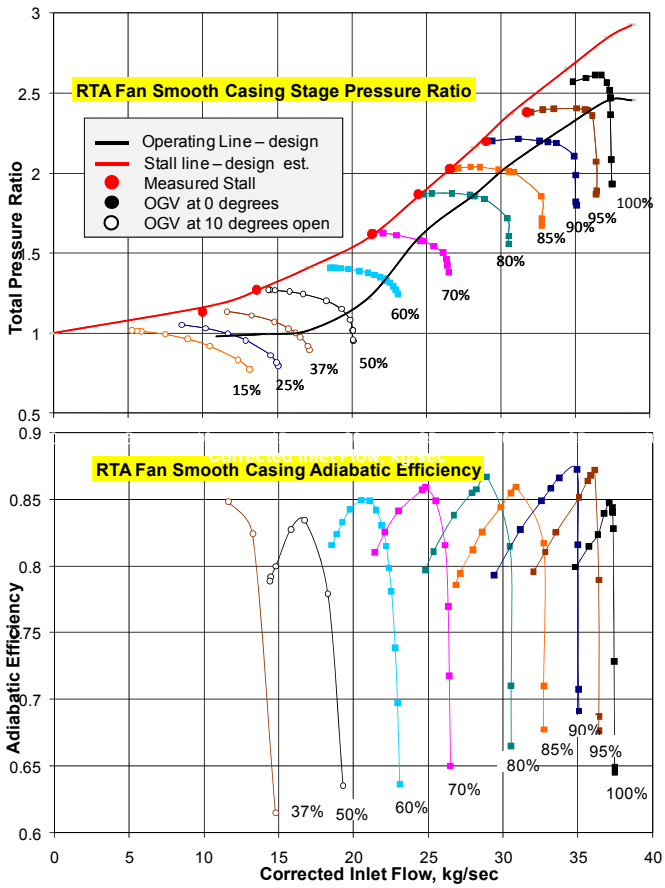

Figure 8.—Stage operating characteristics for the smooth nominal clearance liner configuration.

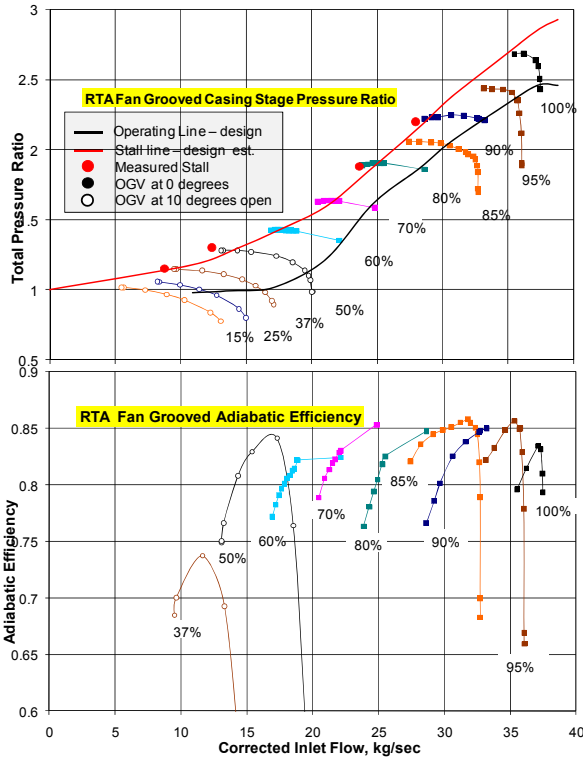

Figure 9.—Stage operating characteristics for the grooved nominal clearance liner configuration.

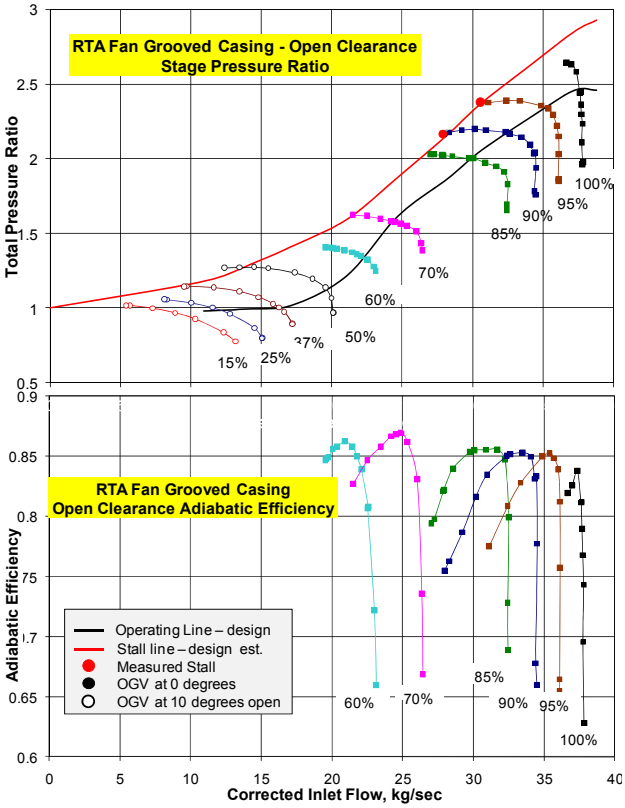

Figure 10.—Stage operating characteristics for the grooved open clearance liner configuration.

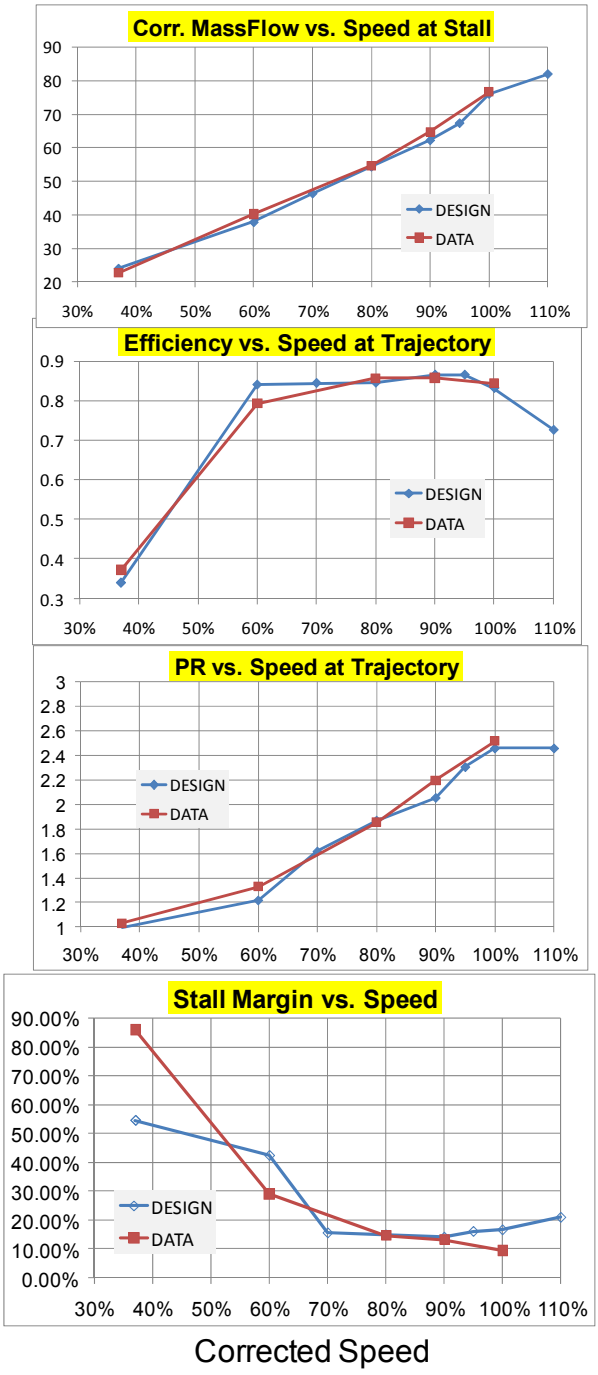

Figure 11.—Comparison of design intent to the measured performance and operability parameters along the operating line for the smooth wall liner configuration.

Sensitivity of Performance to Outer Endwall Configuration

Based on the experimental results presented in Figures 8 to 11 it is evident that the fan stage meets or exceeds the operating line requirements over the entire range of 15 to 100 percent fan speed. (In the companion paper (Ref. 1) of this paper the design intent, experimental data, and APNASA results explicitly show this agreement at 100, 80, and 37 percent speed.) It is also evident that the stall points for the grooved liner configurations occur at a lower operating mass flow than the smooth wall configuration as expected for circumferential groove casing treatment. Furthermore, the maximum flow achieved by the grooved liners configurations is about 1 percent less than the smooth wall configuration for the 70 to 100 percent design speed lines. The sensitivity of the fan stage performance to the 3 liner configurations is more accurately quantified from the plots of stage pressure ratio and adiabatic efficiency at 90 percent speed presented in Figure 12. Note the last data point is at the near stall point and the data missing at the higher flow rate is consistent with the test procedure. The maximum adiabatic efficiency is 2 points higher for the smooth wall configuration at the higher flow rate near the operating line consistent with the higher pressure ratio. However, from the operating line towards the stall line the efficiency is nearly the same for the grooved and smooth wall liners. Though not shown explicitly the same results as discussed above for 90 percent speed were observed at 95 percent speed. Figure 13 shows the measured casing static pressure distribution at 90 percent speed (normalized by the inlet total pressure) over the fan tip for the three liner configurations. The casing statics of Figure 13 are consistent with the overall averaged total pressure rise characteristics shown in Figure 12. The static pressure rise is indicative of fan shock location such that at choke conditions the shock is oblique and pulled back in the fan passage such that the shock hits the suction surface near the trailing edge; whereas at near stall the shock is more normal and intersects the suction surface further upstream nearer to the leading edge. The influence of the circumferential grooves on the stability of the fan stage is evidenced by comparing the results in Figures 12 and 13. On the high flow rate side of the characteristic the grooves and open clearance act as a blockage and reduce the choking flow rate as evidenced by the same fan exit pressure at a much lower flow rate for the grooved liners. In other words the effect of the grooves at higher flow rates requires the fan to operate at a lower flow (higher incidence) to obtain the same fan exit pressure. Comparing results at near stall conditions, the shock for the grooved liner with open clearance is forward of the rotor leading edge, yet the fan stage is not stalled; whereas for the smooth liner configuration the shock is well within the passage and on the verge of stall at a higher flow rate relative to the grooved liner near stall flow rate. Therefore, to summarize, the relief provided by the grooves to enable lower flow rates and more

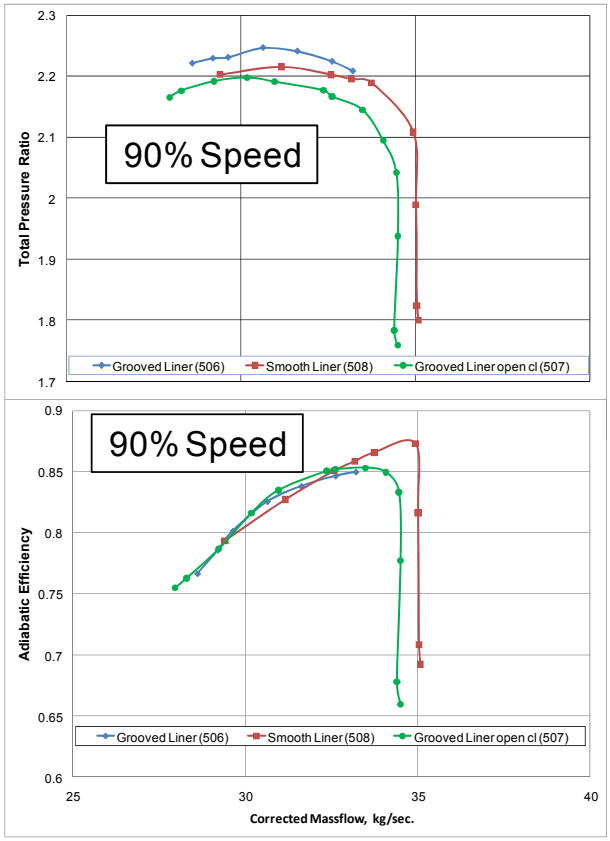

Figure 12.—Comparison of stage pressure ratio and adiabatic efficiency at 90 percent speed for the 3 liner configurations.

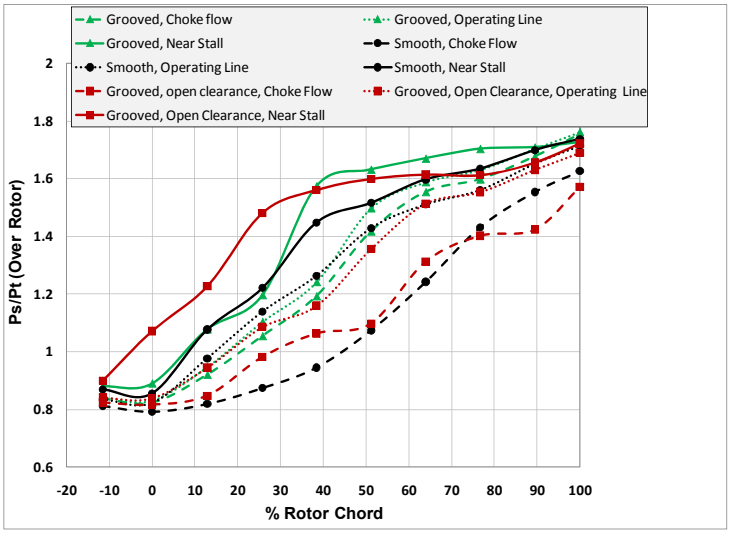

Figure 13.—Comparison of normalized fan tip static pressure distribution for the 3 liners tested at 90 percent speed.

stability margin at near stall operation is offset by increased blockage (resulting in a reduction of the maximum flow) and a lower efficiency at higher flow rates.

The mass flow, pressure ratio, and efficiency along the operating line are tabulated and compared to the corresponding conditions at stall for each of the liner configurations in Table 3. The stall margin is calculated with the operating line condition selected as the reference condition using the standard NASA definition of the stall margin:

$$\text{Stall margin} = \left(\frac{\text{PR @ stall}}{\text{Mass flow @ stall}} \times \frac{\text{Mass flow @ ref}}{\text{PR @ ref}} - 1 \right)$$

TABLE 3.—SUMMARY OF TIP CLEARANCE AND ENDWALL TREATMENT ON STAGE PERFORMANCE AND OPERABILITY

Smooth Wall - nominal Clearance = 0.012" at 100% speed					
DATA	100%	90%	80%	50%	37%
Flow (lbm/sec)	82.5	71.84	62.24	45.63	38.3
PR	2.41	2.2	1.855	1.17	1.03
Efficiency	0.828	0.849	0.857	0.815	0.372
Stall Flow	79.14	64	53.9	30.72	22.3
Stall PR	2.6	2.2	1.87	1.264	1.139
StallMargin (%)		12.6	15.5		

Not Stalled

90% Speed Stall Margin

80% speed Stall Margin

grooved nominal clearance = 0.012" at 100%speed						
DATA	100%	95%	90%	80%	50%	37%
Flow (lbm/sec)	82.6	78.77	72.16	63.1	46.03	39.2
PR	2.432	2.35	2.22	1.859	1.157	1.015
Efficiency	0.793	0.85	0.848	0.848	0.762	0.199
Stall Flow	78.26	73.05	61.6	52.1	27.7	19.74
Stall PR	2.68	2.44	2.222	1.88	1.264	1.138
StallMargin (%)			17.1	22		

Grooved open clearance = 0.045" at 100% speed					
DATA	101%	95%	90%	50%	37%
Flow (lbm/sec)	82.96	78.04	71.9	43.16	35.8
PR	2.442	2.335	2.167	1.133	1.003
Efficiency	0.812	0.852	0.851	0.599	0.039
Stall Flow	80.87	67.4	61.5	27.38	21.01
Stall PR	2.64	2.376	2.165	1.27	1.144
StallMargin (%)			16.9		

Recall from the section describing the test procedure that the fan stage was only throttled to stall for a select few operating conditions. From Table 3 it is apparent that the grooved liners increase the stall margin by 5 to 6 percent at 80 to 100 percent speed, which is typical for circumferential groove casing treatments. For the grooved liner configurations at 100 percent speed, where the clearance varied from 0.012 to 0.045 in., the stall margin and efficiency was nearly identical; thereby, indicating that at the higher loaded conditions, there is little sensitivity to clearance. (Note that aside from the fan tip clearance the two grooved liner configurations were identical.) Below 70 percent fan speed there was virtually no difference measured in fan stage performance and operability for the 3 different liner configurations.

Sensitivity of OGV to Stage Performance and Operability

Static pressure taps on both the suction and pressure surface of the OGV were located at 10, 15, 25, and 45 percent span from the hub of the OGV to monitor the loading of the OGV in the core duct. To assess the loading and incidence as well as determine if the duct was choked the static taps were used to calculate an isentropic relative Mach number using the total pressure at the OGV leading edge. The results for the 37, 60, 80, 90, and 100 percent speed operation are depicted in Figure 14. Note the OGV setting angle was open to 10° at 37 percent speed condition to avoid the OGV leading edge separation and resulting blockage as predicted in the design as seen in Figure 4. At 37 and 60 percent speed along the operating line the stagnation streamline falls well on the suction surface of the OGV possibly resulting in acceleration around the leading edge to the pressure surface and potential separation and increased blockage as shown in Figures 4 and 5. Note that at 100 percent speed the Mach number is nearly one along the suction surface and is indicative of higher OGV losses. Similarly, at 90 percent speed the Mach number is above 0.8 over much of the suction surface. Though not shown at 10 percent span and 100 percent speed the suction surface Mach number is above Mach 0.8 over 75 percent of the OGV chord and exceeds Mach 1 over the first 20 percent of the OGV chord length. Therefore at design speed the OGV passage is potentially choked in the lower spans. In conclusion these Mach number distributions are consistent with the design-predicted trends in OGV incidence and loading from 37 to 100 percent speed.

To further show the sensitivity to OGV incidence and Mach number and clearly demonstrate the necessity for a variable OGV, the Mach number distribution at 60 percent speed for the OGV at 0°, 5°, and 10° is presented in Figure 15. At the design setting of 0° the flow is incident on the suction side and the Mach number approaches 1; whereas at 10° open the flow is better aligned with the OGV leading edge and the Mach number over the suction surface is much reduced. At the lower spans the results (not shown) show a much larger mismatch at the OGV leading edge indicating the OGV needs to swing more than 10° to obtain a near zero incidence along the operating line. With regards to the overall performance, the total pressure ratio maps at 50 and 37 percent speed are plotted in Figure 16 for the baseline OGV setting angle of 0° as well for 5° and 10° open. These results, shown in Figure 16, show an increase in flow rate and increase in stage pressure rise for a given flow rate over most of the operating range. As already mentioned there is no effect of the liner configuration on stage pressure rise below 70 percent speed. In summary these results indicate there is a need for a variable OGV to match the wide swings in incidence and inlet Mach number over the wide operating range and the OGV (not the fan) is the airfoil most sensitive to variations in stage performance over this operating range.

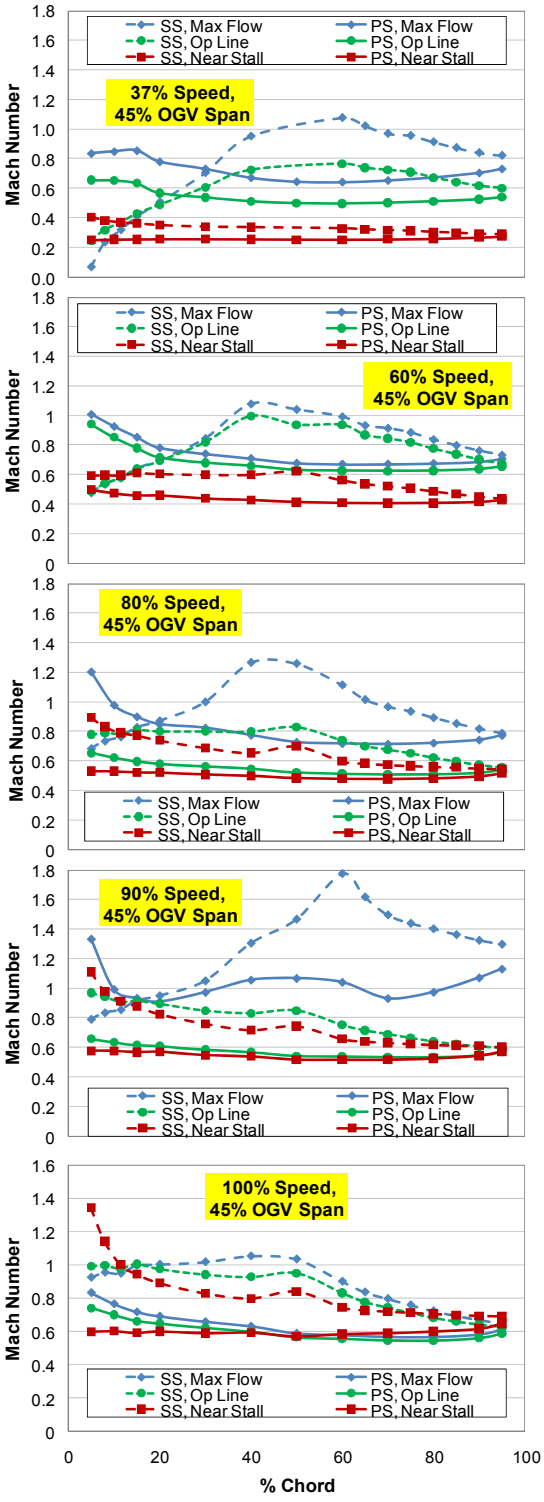

Figure 14.—OGV surface isentropic Mach number values for the smooth wall nominal clearance liner configuration at 45 percent span for 37 to 100 percent speed.

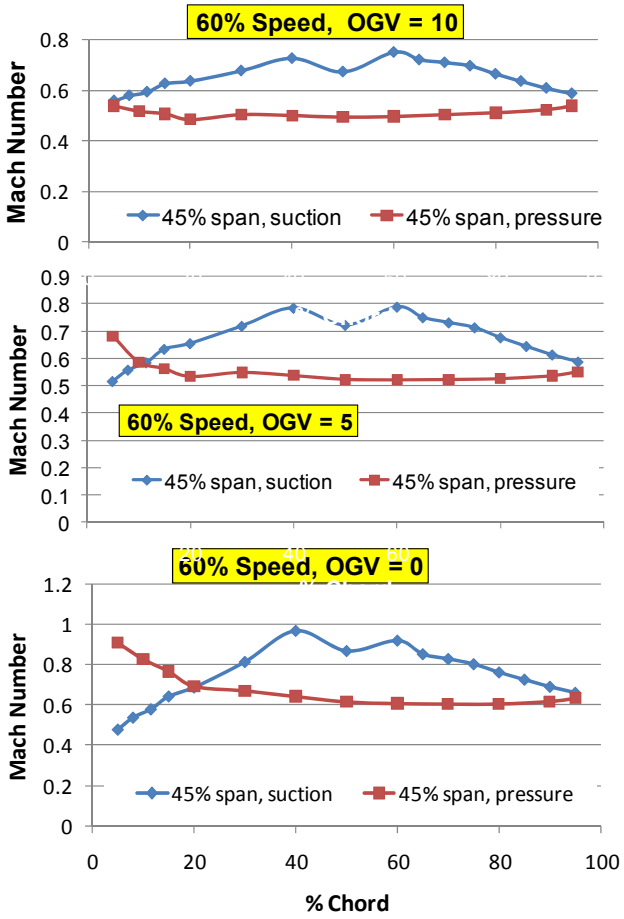

Figure 15.—Effect of OGV setting angle on isentropic Mach number distribution at 60 percent speed.

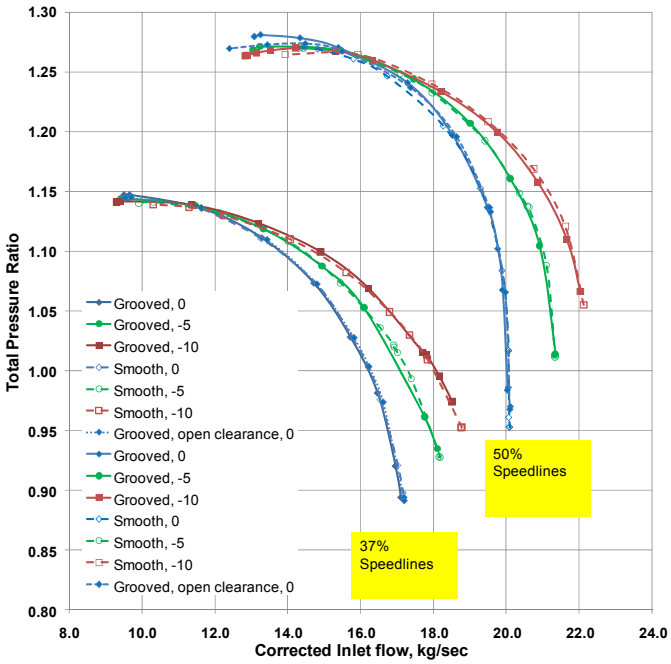

Figure 16.—Sensitivity to stage pressure ratio and mass flow to OGV setting angle at 37 and 50 percent speed.

The stage performance is very sensitive to OGV setting angle as depicted in Figures 14 to 16. Herein we will look at the results for 100 percent speed. Radial distributions of total pressure ratio at the OGV leading edge and downstream rake location (see Fig. 7) as the rotor is back-pressured from choke to stall is plotted in Figure 17. These results indicate as the stage is throttled nearly all of the increase in pressure occurs in the outer spans (beyond point B in the map). In addition there is evidence that the flow is actually choked in that the pressure ratio at about 40 percent immersion does not change with backpressure (also indicated by OGV surface statics). Note the total loss coefficient is defined as the difference in total pressure across the OGV divided by the OGV inlet dynamic pressure. Most surprising is the level of loss coefficient across the entire span greatly exceeding typical values of 0.02 to 0.2 found in traditional OGV designs. These higher losses are due in part to the higher inlet Mach numbers (refer to Fig. 14) which result in higher losses in the OGV across the span and not just at the endwalls. The losses are also in part due to the inherent compromise in performance to provide operability over such a large range but also reflect the slight mismatch between the fan and OGV. Any separations in the OGV are exacerbated by the rapid diffusion downstream of the OGV in the flow path (see Fig. 7) which was necessary to achieve the large swings in bypass ratio required by the cycle deck to meet mission requirements. These results are consistent with the sensitivity of the OGV to separation as it undergoes large swings in incidence and loading. Note that the loss coefficient plot was truncated at 0.5 to show the distribution of loss near the operating line and towards stall. The maximum total loss coefficient reached 1.4 in the hub for the wide open throttle setting and was due to massive separations in the lower spans of the OGV. Though wide open throttle is not an important operating condition, the loss variation in Figure 17 substantiates the sensitivity of stage performance to the OGV inlet conditions. In summary, these results show the sensitivity of the stage performance to OGV inlet conditions and indicate there is a slight mismatch between the OGV and fan over the wide operating range. The pre-test CFD is further investigated to shed insight into the reasons for this mismatch and exceedingly high losses in the OGV especially at 100 percent speed.

Comparison of Data to Pre-Test CFD Using APNASA

As was shown in the section on the fan stage design both NASA and GE CFD codes were used to assess the design as well as to provide input to the design system compressor maps. In this section we will discuss these pre-test CFD simulations using the NASA code APNASA. APNASA (Ref. 9) is a multistage analysis code which provided the ability to analyze the complete fan stage consisting of the fan rotor, OGV, and splitter/strut mid-frame assembly (see Fig. 1).

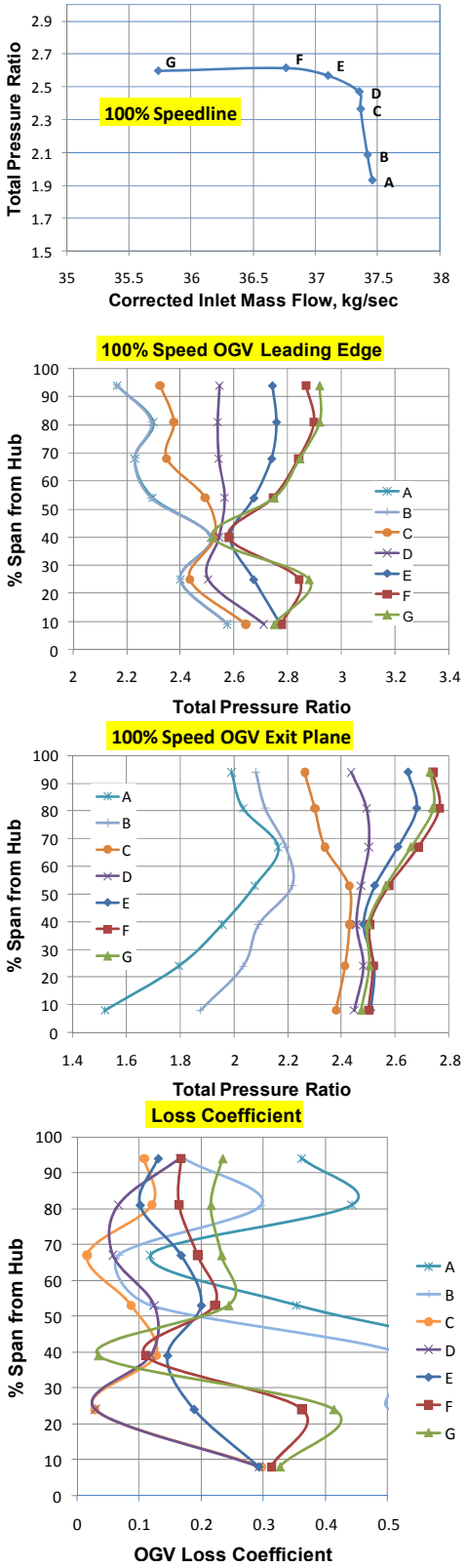

Figure 17.—Radial distributions of total pressure ratio and loss coefficient across the OGV at 100 percent speed.

This approach is unique from 'typical' single passage codes that solve for one blade row at a time by systematically marching through the compression system blade row by blade row utilizing averaged or mixed-out solutions from the upstream blade row as input to the downstream blade row. APNASA solves for the entire flow field. The APNASA fan stage simulation includes body force terms to represent the effect of the downstream OGV and splitter/strut. Similarly the OGV solution includes body-force terms to account for the upstream fan rotor and the downstream strut/splitter, respectively. The numerical procedure solves the three-dimensional Reynolds averaged Navier-Stokes and energy equations using the four step Runge-Kutta scheme and is described by Adamczyk et al. (Ref. 9). The standard two-equation κ–ε model was used to calculate the turbulent eddy viscosity coefficient as described by Shabbir et al. (Refs. 11 and 12). Spalding's formula (Ref. 13) was used to set the wall boundary conditions for the mean flow equations as well as the turbulence model. The inlet boundary conditions consisted of radial profiles of total pressure, total temperature, radial and tangential flow angle which were provided by GE from their design code. The flow in the clearance gap was simulated using a model suggested by Kirtley et al. (Ref. 14).

APNASA results for the overall stage pressure ratio and adiabatic efficiency are compared to the experimental results of the fan stage characteristics at 80, 85, 90, 95, and 100 percent of rotor design speed in Figure 18. The solid symbols represent the data and the open symbols connected by a line indicate the CFD results. Note that only at 100 and 80 percent speed was the CFD simulations back-pressured until they reached their stability limit indicative of an aerodynamic stall point. In general the CFD compared favorably with the data along the operating line both in terms of mass flow, pressure ratio, and to a lesser degree with the efficiency. The major concern for the CFD was the inability of the CFD to predict the stall margin at 100 percent design speed; whereas at 80 percent speed the stall margin was well predicted.

Additional analysis of the CFD at 100 percent speed indicated that if the rotor was back-pressured beyond the operating point at 100 percent speed, the flow in the lower 50 percent span in the OGV became highly separated (due to the higher incidence) and as it was further diffused, the low momentum region grew rapidly and would not allow the CFD simulation to converge. These analyses are presented in Figure 19. CFD simulations were run on the fan rotor only and since the OGV was not in the flow-path the separation did not occur and the fan rotor could be back-pressured such that the stall margin was comparable to that of the measured stage data. These fan only simulations provided confirmation that the separation in the OGV, as predicted by the CFD for the stage configuration, was the reason the operating range at 100 percent speed did not compare well with the data. Due to the sensitivity of the OGV loading and losses with incidence angle and backpressure (discussed in detail in the Experimental Results section), it was recognized that a mass

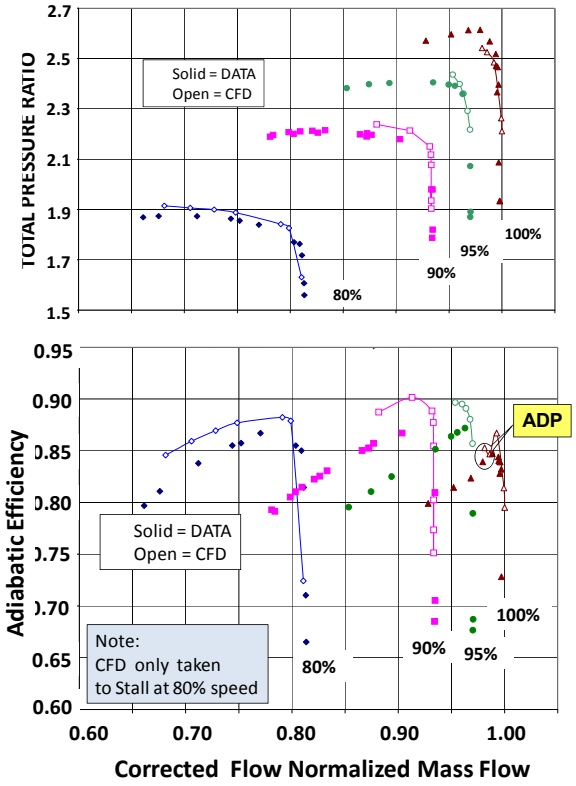

Figure 18.—Comparison of pre-test CFD predictions compared to measured data at 80 to 100 percent speed.

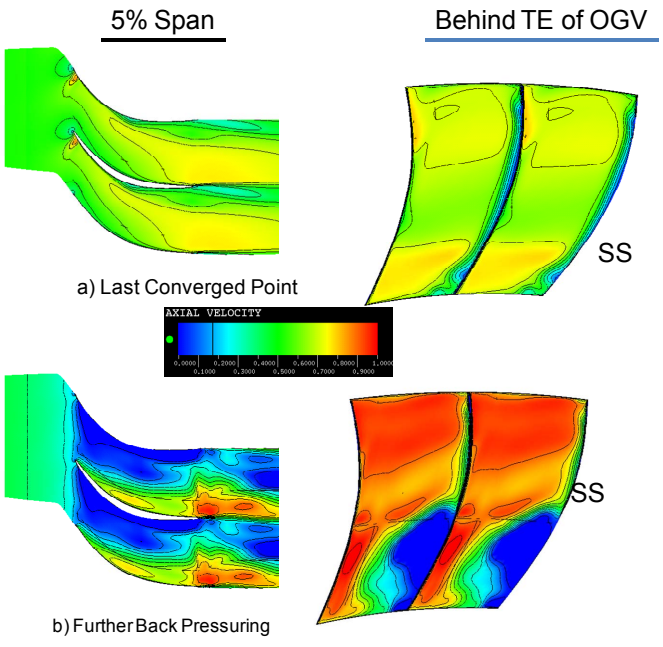

Figure 19.—Pre-test APNASA CFD results at 100 percent speed obtained by setting downstream pressure in the core and bypass ducts.

flow boundary condition must be implemented in the code to enable the CFD simulation to obtain the mass flow and bypass ratio demonstrated in the experimental data obtained away from the operating line. Further analysis of the CFD simulations as well as comparisons with the experimental results led to the conclusions that the CFD did not utilize the same blade geometry or boundary conditions consistent with the experimental data. Therefore, in the companion paper (Ref. 1), we will provide a detailed description of these discrepancies and will perform post-test CFD to assess NASA's APNASA code's ability to predict the fan stage performance and operability over a wide range of speed and bypass ratio.

Summary and Concluding Remarks

The fan stage from a state of the art Mach 4 turbine engine was scaled (57.3 percent linear scale), fabricated, and tested in the NASA W8 Single Stage Compressor facility. The fan stage was designed for multi-point operation to accommodate variations in bypass ratio (10×), fan rotor speed (7×), inlet mass flow (3.5×), inlet pressure (8×), and inlet temperature (3×). Aerodynamic fan stage performance characteristics at 15, 25, 37, 50, 60, 70, 80, 85, 90, 95, and 100 percent of rotor design speed, encompassing a bypass ratio swing from 0.7 to 7, were acquired. These experimental results of the fan stage characteristics were acquired for three different fan rotor casing configurations corresponding to 1) smooth wall at nominal fan tip clearance, 2) circumferentially grooved casing at nominal tip clearance, and 3) circumferentially grooved casing with a more open clearance. The liner influenced the stage performance and operability for fan speeds greater than 70 percent speed, but no influence was measureable below 70 percent speed. At 90 to 100 percent speeds, the relief provided by the grooves to enable lower flow rates and more stability margin at near stall operation was offset by increased blockage (resulting in a reduction of the maximum flow) and a lower efficiency at higher flow rates. The experimental data agreed favorably with the design intent in terms of pressure ratio, efficiency and mass flow along the operating line. It was shown that the OGV loading and losses were sensitive to OGV setting angle and that a variable OGV was required to match the swings in incidence and inlet Mach number over the wide operating range. Furthermore, it was shown that the OGV (not the fan) is the airfoil most sensitive to variations in stage performance over this wide operating range.

Pre-test CFD simulations were integral to the design effort and the results compared very well to the experiment along the design operating line. However, there was some discrepancy between the data and CFD in pressure ratio and adiabatic efficiency at off-design conditions. Most alarming was the fact that the pre-test CFD did not predict the stall margin at 100 percent speed. Inspection of the hardware and analysis of the data revealed the pre-test CFD did not have the corrected hot geometry blade shape and was run at a much larger fan tip clearance than the experiment. Furthermore, the experimental data and pre-test CFD results were obtained at different bypass ratios along the speed-lines for all data points other than for the bypass ratio that was specified in the design along the operating line for each fan speed. These discrepancies between the boundary conditions and input parameters measured in the experiment versus those used for the pre-test CFD predictions, necessitated additional post-test CFD simulations for detailed comparisons between the CFD simulations and experiment which will be presented in Part 2 of this paper (Ref. 1).

The future work will include additional testing and analysis to assess sensitivity of performance and operability to both endwall variations and inlet flow distortions. The distortion measured from the TBBC large scale inlet described in References 15 to 17 will be simulated with distortion screens at the inlet of the fan stage. The data will be used to evaluate the impact of distortion on the fan stage performance and operability as well as be used to assess the ability of the SOA tools to predict these effects. For non-axisymmetric inlet distortions unsteady analysis codes will need to be used. Therefore, studies have begun to baseline a full unsteady simulation by comparing the predictions of the unsteady codes (for the uniform inlet flow data presented herein) to those of APNASA's averaged passage results presented in the companion paper (Ref. 1) to this paper.

References

1. Celestina, M.L., Suder, K.L., and Kulkarni, S. 2010, "Results of an Advanced Fan Stage Operating Over a Wide Range of Speed & Bypass Ratio—Part 2: Comparison of CFD and Experimental Results," ASME Paper No. GT2010–23386, 2010.
2. Bilardo V.J., Curran F.M., Lovell N.T., and Maggio G., 2003, "Benefits of Airbreathing Launch Systems for Access to Space," AIAA–2003–5265, 39th Joint Propulsion Conference in Huntsville, Alabama, July 20–23, 2003.
3. Shafer D.G., McNelis N., 2003, "Development of a Ground Based Mach 4+ Revolutionary Turbine Accelerator Technology Demonstrator (RTATD) for Access to Space," ISOABE 2003.
4. "RTA Propulsion System Data Requirements/Boeing TSTO Study from NASA Glenn," RASER Contract NAS3-01135, 2002.
5. Mielke, M., Clark, D., and Wood, P. 2009 "RTA/GE57 Subscale Fan Rig, Final Report—Aero & Aeromechanical," NASA/CR—2010-215815.
6. Suder, K.L., Adamczyk, J.A, Wood, p., 2005 "Design and Analysis of a Mach 4 Capable Fan Stage for the RTA Turbine Based Combined Cycle Propulsion System," JANNAF (Joint Army, Navy, NASA, Air Force) 42nd

CS/30th APS/24th PSHS Joint Meeting, Charleston, SC June, 2005.
7. Mielke, M., 2009 "RTA/GE57 Subscale Fan Rig, Final Report—Mechanical Design," NASA/CR—2010-215814.
8. Smith, L.H. and Yeh, H., 1963, "Sweep and Dihedral Effects in Axial-Flow Turbomachinery," ASME Journal of Basic Engineering, Vol. 85, pp. 401–416.
9. Adamczyk, J.J., Celestina, M.L., Beach, T.A., and Barnett, M., 1990," Simulation of Three-dimensional Viscous Flow within a Multistage Turbine," Tran. ASME, 112, 370–376.
10. Mielke, M., Clark, D., and Wood, P. 2009 "RTA/GE57 Subscale Fan Rig, Final Report—Aerodynamic Test Results," NASA/CR—2009-215816.
11. Shabbir, A. and Turner, M.G., 2004, "A Wall Function for Calculating the Skin Friction With Surface Roughness," A. Shabbir and M.G. Turner, ASME Paper GT2004–53908.
12. Shabbir, A., Zhu, J., and Celestina, M.L. 1996, "Assessment of the Three-Dimensional Models in a Compressor Rotor," ASME Paper No. 96-GT-1998.
13. Spalding, D.B., 1961, "A Single Formula for the Law of the Wall," J. Appl Mech. 28, pp. 455–458.
14. Kirtley, K.R., Beach, T.A., and Adamczyk, J.J., 1990, "Numerical Analysis of Secondary Flow in a Two-Stage Turbine," Paper no. AIAA–90–2356.
15. Sanders, B.W.; and Weir, L.J.: "Aerodynamic Design of a Dual-Flow Mach 7 Hypersonic Inlet System for a Turbine-Based Combined-Cycle Hypersonic Propulsion System," NASA/CR—2008-215214, May 2008.
16. Auslender, A.H., Suder, K.L., Thomas, S.R.: "An Overview of the NASA FAP Hypersonics Project Airbreathing Propulsion Research, 16th AIAA/DLR/DGLR International Space Planes and Hypersonic Systems and Technologies Conference, AIAA–2009–7277, October 2009.
17. Suder, K.L., Thomas, S.R., "An Overview of the NASA Hypersonic Project's Combined Cycle Engine Mode Transition Research Experiment," JANNAF (Joint Army, Navy, NASA, Air Force) 44th CS/32th APS/26th PSHS Joint Meeting, La Jolla, CA, December 7–11, 2009.

REPORT DOCUMENTATION PAGE			Form Approved OMB No. 0704-0188

The public reporting burden for this collection of information is estimated to average 1 hour per response, including the time for reviewing instructions, searching existing data sources, gathering and maintaining the data needed, and completing and reviewing the collection of information. Send comments regarding this burden estimate or any other aspect of this collection of information, including suggestions for reducing this burden, to Department of Defense, Washington Headquarters Services, Directorate for Information Operations and Reports (0704-0188), 1215 Jefferson Davis Highway, Suite 1204, Arlington, VA 22202-4302. Respondents should be aware that notwithstanding any other provision of law, no person shall be subject to any penalty for failing to comply with a collection of information if it does not display a currently valid OMB control number.
PLEASE DO NOT RETURN YOUR FORM TO THE ABOVE ADDRESS.

1. REPORT DATE *(DD-MM-YYYY)*	2. REPORT TYPE	3. DATES COVERED *(From - To)*
01-10-2011	Technical Memorandum	

4. TITLE AND SUBTITLE
Results of an Advanced Fan Stage Operating Over a Wide Range of Speed and Bypass Ratio
Part I: Fan Stage Design and Experimental Results

5a. CONTRACT NUMBER

5b. GRANT NUMBER

5c. PROGRAM ELEMENT NUMBER

6. AUTHOR(S)
Suder, Kenneth, L.; Prahst, Patricia, S.; Thorp, Scott, A.

5d. PROJECT NUMBER

5e. TASK NUMBER

5f. WORK UNIT NUMBER
WBS 599489.02.07.03.07

7. PERFORMING ORGANIZATION NAME(S) AND ADDRESS(ES)
National Aeronautics and Space Administration
John H. Glenn Research Center at Lewis Field
Cleveland, Ohio 44135-3191

8. PERFORMING ORGANIZATION REPORT NUMBER
E-17395-1

9. SPONSORING/MONITORING AGENCY NAME(S) AND ADDRESS(ES)
National Aeronautics and Space Administration
Washington, DC 20546-0001

10. SPONSORING/MONITOR'S ACRONYM(S)
NASA

11. SPONSORING/MONITORING REPORT NUMBER
NASA/TM-2011-216769-PART1

12. DISTRIBUTION/AVAILABILITY STATEMENT
Unclassified-Unlimited
Subject Category: 02
Available electronically at http://www.sti.nasa.gov
This publication is available from the NASA Center for AeroSpace Information, 443-757-5802

13. SUPPLEMENTARY NOTES

14. ABSTRACT
NASA's Fundamental Aeronautics Program is investigating turbine-based combined cycle (TBCC) propulsion systems for access to space because it provides the potential for aircraft-like, space-launch operations that may significantly reduce launch costs and improve safety. To this end, National Aeronautics and Space Administration (NASA) and General Electric (GE) teamed to design a Mach 4 variable cycle turbofan/ramjet engine for access to space. To enable the wide operating range of a Mach 4+ variable cycle turbofan ramjet required the development of a unique fan stage design capable of multi-point operation to accommodate variations in bypass ratio (10×), fan speed (7×), inlet mass flow (3.5×), inlet pressure (8×), and inlet temperature (3×). In this paper, NASA has set out to characterize a TBCC engine fan stage aerodynamic performance and stability limits over a wide operating range including power-on and hypersonic-unique "windmill" operation. Herein, we will present the fan stage design, and the experimental test results of the fan stage operating from 15 to 100 percent corrected design speed. Whereas, in the companion paper, we will provide an assessment of NASA's APNASA code's ability to predict the fan stage performance and operability over a wide range of speed and bypass ratio.

15. SUBJECT TERMS
Fan stage; Compressor rotor

16. SECURITY CLASSIFICATION OF:			17. LIMITATION OF ABSTRACT	18. NUMBER OF PAGES	19a. NAME OF RESPONSIBLE PERSON
a. REPORT	b. ABSTRACT	c. THIS PAGE			STI Help Desk (email:help@sti.nasa.gov)
U	U	U	UU	21	19b. TELEPHONE NUMBER *(include area code)* 443-757-5802